AIP | Applied Physics Letters

Bending stiffness and interlayer shear modulus of few-layer graphene

Xiaoming Chen, Chenglin Yi, and Changhong Ke

Citation: Applied Physics Letters **106**, 101907 (2015); doi: 10.1063/1.4915075
View online: http://dx.doi.org/10.1063/1.4915075
View Table of Contents: http://scitation.aip.org/content/aip/journal/apl/106/10?ver=pdfcov
Published by the AIP Publishing

Bending stiffness and interlayer shear modulus of few-layer graphene

Xiaoming Chen, Chenglin Yi, and Changhong Ke[a)]
Department of Mechanical Engineering, State University of New York at Binghamton, Binghamton, New York 13902, USA

(Received 9 December 2014; accepted 3 March 2015; published online 11 March 2015)

Interlayer shear deformation occurs in the bending of multilayer graphene with unconstrained ends, thus influencing its bending rigidity. Here, we investigate the bending stiffness and interlayer shear modulus of few-layer graphene through examining its self-folding conformation on a flat substrate using atomic force microscopy in conjunction with nonlinear mechanics modeling. The results reveal that the bending stiffness of 2–6 layers graphene follows a square-power relationship with its thickness. The interlayer shear modulus is found to be in the range of 0.36–0.49 GPa. The research findings show that the weak interlayer shear interaction has a substantial stiffening effect for multilayer graphene. © *2015 AIP Publishing LLC*. [http://dx.doi.org/10.1063/1.4915075]

The mechanical properties of graphene, which is composed of two-dimensional honeycomb carbon lattice networks, are of importance in the pursuit of many of its potential applications, such as graphene-based nanoelectromechanical resonators[1] and switches,[2] and programmable building blocks or origami.[3–6] For monolayer graphene, its bending rigidity originates from stretching and compression of covalent carbon-carbon bonds that occur as a result of its out-of-plane deformation.[7,8] For multilayer graphene, its bending rigidity depends not only on its thickness or number of graphene layers (N) but also the interlayer shear interaction. Based on classic continuum mechanics theories, the bending stiffness of a laminated beam consisting of N identical beam elements is expected to be within N to N^3 times that of individual beam elements. The lower bound corresponds to free or zero shear interactions between adjacent layers, while the upper bound corresponds to a perfectly bonded interface and thus no interlayer sliding between adjacent layers. Therefore, the interlayer shear rigidity in multilayer graphene is expected to have a substantial influence on its bending rigidity and other related physical properties (e.g., natural frequency). The neighboring graphene sheets interact with each other via van der Waals (vdW) interactions. Compared to the strong in-plane rigidity of individual graphene sheets, interlayer shear rigidity in multilayer graphene is fairly weak such that the registry of carbon atoms in the adjacent graphene layers cannot be maintained, and thus interlayer shear deformation occurs under even modest shear loadings[9] or bending deformations.[10] In spite of the substantial advances in the study of mechanical properties of graphene in the past few years, the bending and interlayer shear rigidities of multilayer graphene remain not well understood. A majority of the reported studies on graphene's bending and interlayer shear rigidities are based on theoretical modeling,[10–14] while the experimental data reported in the literature remain limited.[9,15–17] Notably, the bending stiffness of mono- to trilayer graphene was previously investigated using electrostatic bending methods.[15] The bending stiffness of relatively thick graphene ($N \geq 8$) was investigated using atomic force microscopy (AFM)-based nanoindentation techniques.[18] For both studies, the tested graphene sheets were under both bending and stretching deformations due to the imposed doubly-clamped boundary conditions, and thus the measured graphene bending stiffness might be substantially influenced by the stretching effect.

In this study, we investigate the bending and interlayer shear rigidities of few-layer graphene through measuring its self-folding conformation on a flat substrate using high resolution AFM in conjunction with nonlinear mechanics modeling. Due to their low bending rigidities, it is energetically favorable for thin graphene sheets to form stable self-folding configurations on a substrate via graphene-graphene and graphene-substrate vdW interactions.[12,19,20] The folding curvature of the graphene reflects its overall bending resistance to the adhesion interactions. Our studies reveal that the bending stiffness of two to six layers graphene follows a square-power relationship with its thickness. The interlayer shear rigidity and modulus are quantified using energy method.

The graphene sheets employed in this study were obtained through mechanically exfoliating highly ordered pyrolytic graphite (HOPG) films.[21] After transferring to flat silicon oxide (SiO_2) substrates, some graphene flakes were found to stay in self-folded configuration by means of AFM imaging. The AFM measurements were performed inside a Park Systems XE-70 AFM that operates at a tapping mode with silicon AFM tips (nominal tip radius $\sim$ 10 nm). Figure 1(a) shows a representative partially self-folded graphene sheet that was plausibly formed through tearing a stripe of about 30 nm in width. The top panel in Figure 1(a) displays a 3D schematic drawing of the self-folded graphene stripe. It is noted that the formation of the self-folded graphene as shown in Figure 1(a) occurs in an uncontrollable and random manner. We also manufactured self-folded graphene through nanomanipulating originally flat graphene flakes using AFM probes, which is illustrated by the schematic drawings in Figure 1(b). The two AFM images displayed in Figure 1(b) show one graphene before and after folding, respectively. Figure 1(c) shows the respective AFM line topography profiles of the same spot on the unfolded and folded graphene shown in Figure 1(b), which are marked in

[a)]Author to whom correspondence should be addressed. Electronic mail: cke@binghamton.edu.

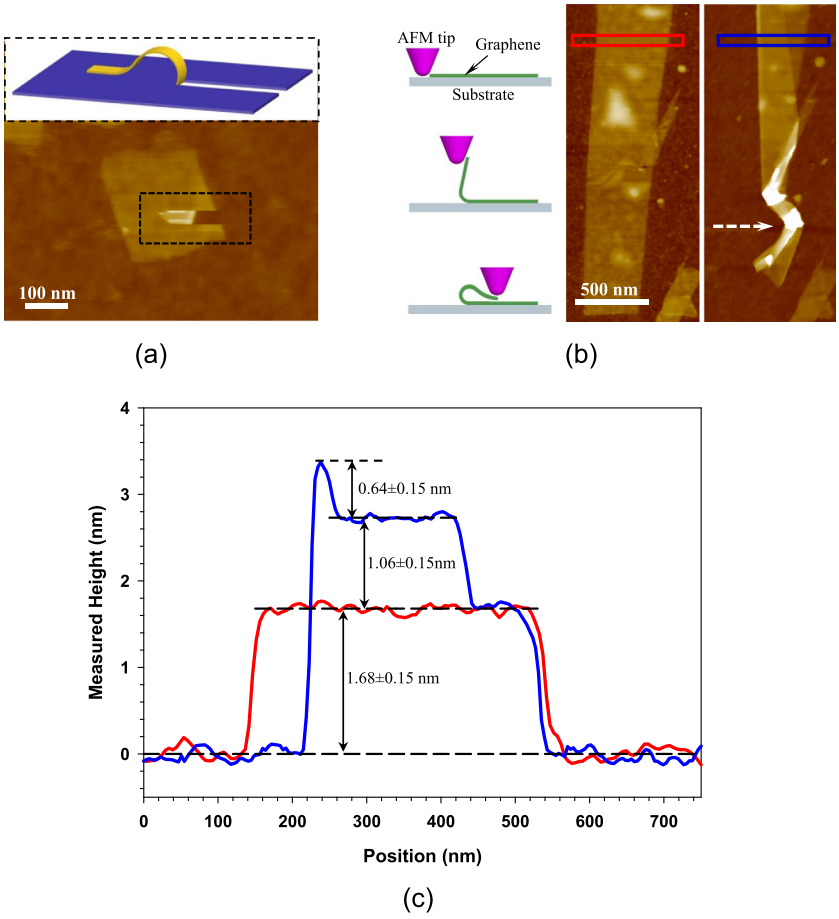

FIG. 1. (a) AFM image of one graphene sheet with a self-folded stripe. The top panel shows a 3D schematic of the folding graphene stripe. (b) (*left*) Schematic drawings of folding a graphene using AFM-based nanomanipulation techniques, and AFM images showing one folded graphene obtained using this approach: original graphene (*middle*) and folded graphene (*right*). The arrow indicates the contact and the movement direction of the AFM probe. (c) AFM line topography profiles of the same graphene before (red curve) and after (blue curve) folding for the areas marked by the red and the blue boxes, respectively.

the red and blue boxes. One prominent step is displayed in the unfolded graphene profile, whose height corresponds to the graphene height on the substrate. For the folded segment, the graphene height measured on top of the unfolded segment (1.06 ± 0.15 nm) is considered as its actual thickness,[20,22,23] which is smaller than the measured height of the unfolded graphene on the substrate (1.68 ± 0.15 nm). The data indicate that the sheet shown in Figure 1(b) is a trilayer graphene that possesses a theoretical thickness of 1.02 nm.[24] The graphene folding edge is exhibited as a hump in its topography profile, and its height is measured to be about 0.64 nm with respect to the top surface of the folded segment.

We have measured and analyzed a number of self-folded graphene flakes, and identified 21 samples that comprise 2–6 layers graphene. The measured step and hump heights of five selected samples are listed in Table I. Figure 2 shows that the dependence of the measured hump height on the number of graphene layers, which can be well-fitted by a linear curve. The results show that the hump height around the folding edge increases nearly linearly with the graphene thickness.

We quantify the overall bending stiffness of graphene based on its self-folding conformation using a nonlinear continuum mechanics model. Figure 3(a) gives a schematic illustration of the nonlinear continuum model for a self-folded graphene on a flat substrate, in which the blue curve represents the middle-plane of the folded graphene. In this model, the graphene is simplified as a solid inextensible elastica beam, and its element is under pure bending deformation. The governing equation for the deformation of the elastica beam is given as[25]

$$\frac{d^2\theta}{ds^2} = \frac{T\sin\theta - V\cos\theta}{D_m}, \tag{1}$$

TABLE I. The key experimentally measured and theoretically calculated parameters of the self-folded graphene (for individual samples), and the calculated graphene's bending stiffness and interlayer shear modulus (for all the tested graphene with the same number of layers). Samples #2 and #5 correspond to the graphene sheets displayed in Figures 1(b) and 1(a), respectively.

#	Step height (G-G) (nm)	Step height (G-SiO_2) (nm)	Hump height (nm)	Assigned number of layers (N)	Number of samples for same type of graphene	Graphene bending stiffness (eV)	Graphene interlayer shear modulus (GPa)
1	0.71 ± 0.15	1.51 ± 0.15	0.48 ± 0.15	2	3	3.35 ± 0.43	0.40 ± 0.25
2	1.06 ± 0.15	1.68 ± 0.15	0.64 ± 0.15	3	7	6.92 ± 0.94	0.49 ± 0.08
3	1.40 ± 0.15	2.01 ± 0.15	0.87 ± 0.15	4	3	12.50 ± 1.34	0.47 ± 0.02
4	1.77 ± 0.15	2.27 ± 0.15	0.93 ± 0.15	5	3	18.10 ± 1.45	0.40 ± 0.01
5	2.11 ± 0.16	2.67 ± 0.16	1.31 ± 0.16	6	5	28.29 ± 2.08	0.36 ± 0.004

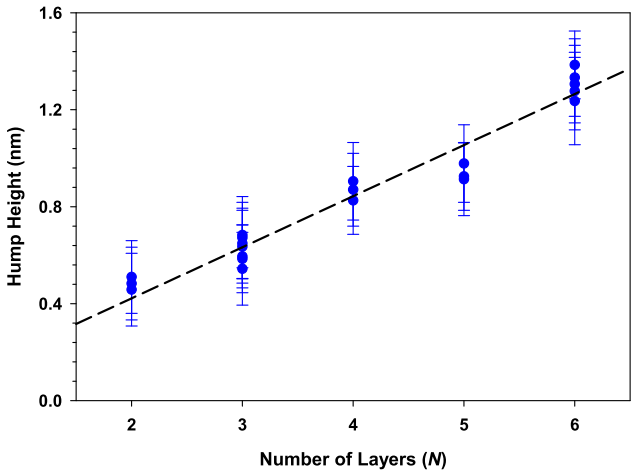

FIG. 2. The measured hump height on self-folded graphene sheets. The dashed line is a linear fitting curve with an R-squared value of 0.95.

where θ is the rotation angle; s is the arc length measured from point A; D_m is the bending stiffness per unit length of the beam; and V and T are the shear force and normal force within the beam, respectively. Positions A ($y = d/2,\ \theta = 0$) and B ($y = -d/2,\ \theta = -\pi$) are two delamination fronts, and their respective bending curvatures, defined as $k = \mathrm{d}\theta/\mathrm{d}s$, are given as $k_A = \sqrt{2\Gamma_g/D_m}$ and $k_B = \sqrt{2\Gamma_s/D_m}$,[26] where Γ_g and Γ_s are the respective adhesion energies per unit area in the flat adhered region, and between the graphene and the substrate. For N-layer graphene, the equilibrium distance $d = N \times t_0$, where $t_0 = 0.34\,\mathrm{nm}$ is the graphene interlayer space. Γ_g is calculated based on the 6–12 Lennard-Jones potential, and is found to be $0.26\,\mathrm{J/m^2}$ (for $N = 2$) and $0.267\,\mathrm{J/m^2}$ (for $N \geq 3$). $\Gamma_s = 0.338\,\mathrm{J/m^2}$ (Ref. 20) is also adopted in the analysis.

We calculate the bending stiffness D_m through fitting the theoretically predicted hump height using Eq. (1) to the measured value. The corresponding deviation error is determined based on the calculated rms value of the measured hump height. Figure 3(b) displays the overall bending stiffness of all measured graphene samples. Our analysis reveals that the dependence of the bending stiffness of few-layer graphene on its thickness can be well fitted by a square-power curve that is given by $D_m(\mathrm{eV}) = 6.7[N \times t_0(nm)]^2$ with an R-squared value of 0.99. The N^2 power relationship indicates that the bending rigidity of multilayer graphene is substantially higher than a simple summation of the bending stiffness of each individual layer, which has been assumed in prior theoretical studies based on continuum mechanics modeling.[27,28] The findings suggest that the strain energy associated with the interlayer shear deformation has a substantial stiffening effect on the bending rigidity of few-layer graphene. Through extrapolation, the power fitting curve yields a value of 0.77 eV for monolayer graphene, which is lower than the reported values (1.0–1.6 eV) obtained by molecular dynamics and *ab initio* calculations,[7,29,30] and the experimental value derived from phonon spectrum of graphite (1.2 eV).[31] The results suggest that monolayer graphene has a different bending mechanism from multilayer graphene. Similar observation has also been documented regarding the bending properties of single- and multi-walled carbon

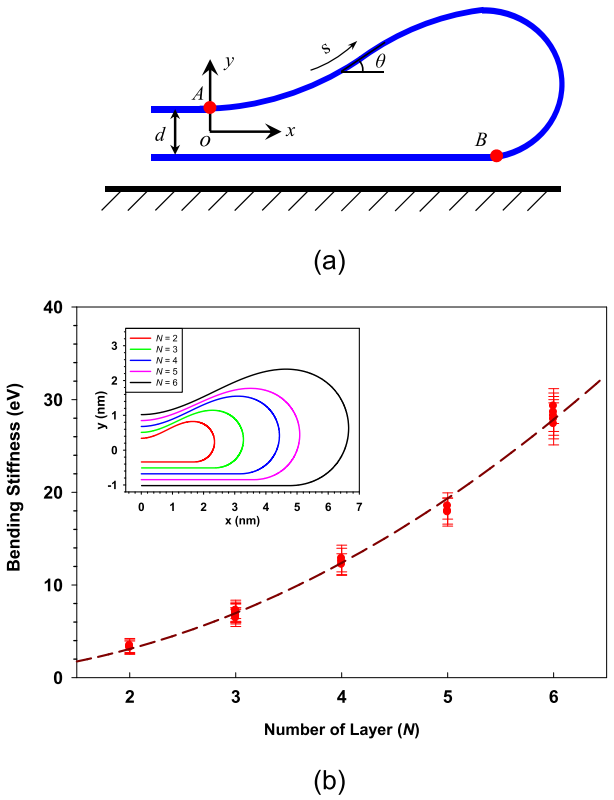

FIG. 3. (a) The nonlinear continuum model of self-folding of graphene on a flat substrate. (b) The calculated bending stiffness based on the measured self-folded graphene. The dashed line is a square-power fitting curve with an R-squared value of 0.99. The inset graph shows the predicted middle-plane profiles of the folded multilayer graphene sheets using Eq. (1) based on the average bending stiffness of each type of graphene listed in Table I.

nanotubes.[32] The average bending stiffnesses of bi- and tri-layer graphene are found to be about 3.35 and 6.92 eV, respectively, which are substantially lower than the reported data obtained on doubly-clamped graphene using electrostatic bending techniques (i.e., 35.5 eV for bilayer and 126 eV for trilayer graphene).[15] The substantial discrepancy can be ascribed to the difference in boundary conditions imposed on the tested graphene in these two studies. The inset graph in Figure 3(b) shows the theoretically predicted self-folding deformation profile (middle plane, curved portion only) for each type of graphene based on its average bending stiffness listed in Table I.

We investigate the interlayer shear rigidity and modulus using energy method based on a multi-beam shear (MBS) model.[10] Here, we illustrate the MBS model using a deformed bilayer graphene element *ABCD* that is depicted as the inset drawing in Figure 4. It is assumed that the deformations of all the graphene layers follow the same geometric shape, and all the interlayer spaces remain intact. *O* is the center of curvature for the deformed element at points *A* and *C* (for simplicity of derivation, here *OAC* is assumed to be a straight line, but the conclusion is also valid without this assumption). The radius of curvature of the inner layer element (*AB*) is given by $r = r(\theta)$, where θ is the angle formed by segments *OA* and *OB*, and is also the slope angle at point *B*. The radius of curvature of the outer layer element (*CD*) equals $r(\theta) + t_0$. *E* is the cross-over point between the extensions of *OB* and *CD*. The shear deformation of the interlayer element *ABCD* is given as

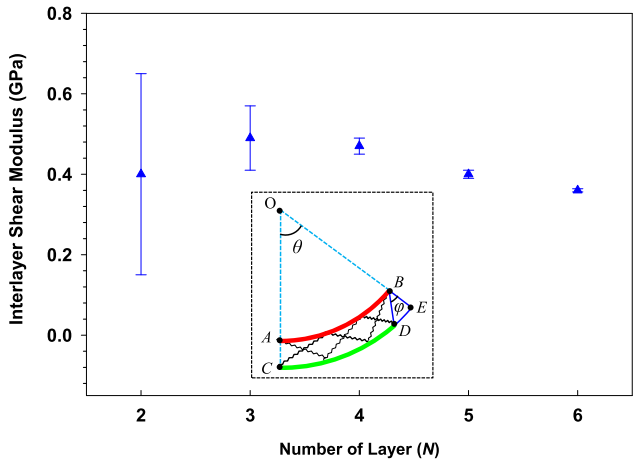

FIG. 4. The calculated interlayer shear modulus based on the measured self-folded graphene. The inset drawing shows the deformation of a bilayer graphene element based on multibeam shear model. The red and green segments illustrate the inner and outer graphene layer elements, respectively. The massless springs represent interlayer shear.

$\varphi = \tan^{-1}(\overline{DE}/\overline{BE})$. The arc lengths of AB and CE can be expressed as $\overline{AB} = \int_0^\theta r(\theta)\,\mathrm{d}\theta$ and $\overline{CE} = \int_0^\theta [r(\theta) + t_0]\,\mathrm{d}\theta$, respectively. Because $\overline{AB} = \overline{CD}$, $\overline{DE} = \overline{CE} - \overline{AB} = t_0 \times \theta$. Therefore, $\varphi = \tan^{-1}(\theta)$. $\varphi \approx \theta$ is valid for small deformation scenarios.[10]

In the MBS model, the total strain energy in the folded graphene is composed of both bending and interlayer shear energies, which are simple summations of the respective energies in each graphene layer and interlayer. The per-unit-length interlayer shear energy, $\mathrm{d}E_G$, can be obtained from the interlayer shear modulus, G, and is given as $\mathrm{d}E_G = \frac{(N-1)Gt_0}{2}(\tan^{-1}\theta)^2\mathrm{d}s$ for N-layer graphene, in which the product of G and t_0 gives the interlayer shear rigidity of unit width. It is noted that the bending energy stored in each graphene layer is different because its bending curvature, denoted as $\kappa_i (i = 1 \text{ to } N)$, varies. The per-unit-length bending energy in N-layer graphene is given as $\mathrm{d}E_B = \frac{D_s}{2}\sum_{i=1}^{N}\kappa_i^2\mathrm{d}s$, where D_s is the bending stiffness of monolayer graphene. In the elastica beam model, the total strain energy equals the bending energy in the multilayer graphene, which is given as $\mathrm{d}E_B^* = \frac{D_m}{2}\kappa^2\mathrm{d}s$ on a per-unit-length basis. Considering an energy balance regarding the total strain energy stored in the folded graphene segment with a length L, we get

$$\frac{D_m}{2}\int_0^L \kappa^2\mathrm{d}s = \frac{D_s}{2}\sum_{i=1}^{N}\int_0^L \kappa_i^2\mathrm{d}s + \frac{(N-1)Gt_0}{2}\int_0^L (\tan^{-1}\theta)^2\mathrm{d}s. \tag{2}$$

The predicted self-folding profiles that are displayed in Figure 3(b) are employed as the shape functions in the calculation of all the integrations in Eq. (2). Thus, the interlayer shear modulus G can be obtained from Eq. (2). $D_s = 1.3$ eV is employed in the analysis. Figure 4 shows the calculated interlayer shear modulus based on the average bending stiffness of each type of graphene. The interlayer shear modulus for 2–6 layers graphene is found to be consistently within the range of 0.36–0.49 GPa. Our data are slightly higher than those reported in the literature that were obtained from *ab initio* (0.19–0.34 GPa)[13] and molecular dynamics (0.25–0.29 GPa)[10,14] studies for graphene with random stacking. Meanwhile, our data are substantially lower than the reported value for graphene/graphite (~5 GPa) with perfect AB stacking.[17,33] These results clearly indicate that the stacking of the graphene layers in the self-folded structure deviates substantially from perfect AB stacking patterns, which can be attributed to the relative sliding of carbon lattices as a result of interlayer shear deformations. It is also noticed that the error bars of the interlayer shear modulus span a larger range for thinner graphene, even though the error bars of the bending stiffness for all types of graphene are comparable on a percentage-wide basis. The observation can be attributed to the fact that the ratio between the numbers of interlayers and graphene layers is smaller for thinner graphene. The interlayer shear energy in thinner graphene accounts for a smaller percentage of the total strain energy. Therefore, the same deviation in the bending stiffness leads to a larger scattering in the quantified interlayer shear modulus for thinner graphene.

In summary, the bending and interlayer shear rigidities of few-layer graphene are investigated. The results reveal that the bending stiffness of 2–6 layers graphene follows a square-power relationship with its thickness. The research findings show that the weak interlayer shear interaction has a substantial stiffening effect on the bending rigidity of multilayer graphene. Therefore, the interlayer shear deformation and the associated strain energy should be taken into account in the studies of mechanical deformations of multilayer graphene. This work is useful in better understanding the structural and mechanical properties of graphene and in the pursuit of its applications, in particular, those involving bending or folding graphene structures.

This work was partially supported by U.S. Air Force Office of Scientific Research under the Grant No. FA9550-11-1-0042.

[1]J. S. Bunch, A. M. van der Zande, S. S. Verbridge, I. W. Frank, D. M. Tanenbaum, J. M. Parpia, H. G. Craighead, and P. L. McEuen, Science **315**, 490 (2007).
[2]K. M. Milaninia, M. A. Baldo, A. Reina, and J. Kong, Appl. Phys. Lett. **95**, 183105 (2009).
[3]S. Zhu and T. Li, ACS Nano **8**, 2864 (2014).
[4]M. Becton, L. Zhang, and X. Wang, Chem. Phys. Lett. **584**, 135 (2013).
[5]L. Zhang, X. Zeng, and X. Wang, Sci. Rep. **3**, 3162 (2013).
[6]V. B. Shenoy and D. H. Gracias, MRS Bull. **37**, 847 (2012).
[7]D.-B. Zhang, E. Akatyeva, and T. Dumitrică, Phys. Rev. Lett. **106**, 255503 (2011).
[8]N. G. Chopra, L. X. Benedict, V. H. Crespi, M. L. Cohen, S. G. Louie, and A. Zettl, Nature **377**, 135 (1995).
[9]X. Feng, S. Kwon, J. Y. Park, and M. Salmeron, ACS Nano **7**, 1718 (2013).
[10]Y. Liu, Z. Xu, and Q. Zheng, J. Mech. Phys. Solids **59**, 1613 (2011).
[11]J. Zhang, J. Xiao, X. Meng, C. Monroe, Y. Huang, and J.-M. Zuo, Phys. Rev. Lett. **104**, 166805 (2010).
[12]X. Meng, M. Li, Z. Kang, X. Zhang, and J. Xiao, J. Phys. Appl. Phys. **46**, 055308 (2013).
[13]G. Savini, Y. J. Dappe, S. Öberg, J.-C. Charlier, M. I. Katsnelson, and A. Fasolino, Carbon **49**, 62 (2011).
[14]Y. Shen and H. Wu, Appl. Phys. Lett. **100**, 101909 (2012).
[15]N. Lindahl, D. Midtvedt, J. Svensson, O. A. Nerushev, N. Lindvall, A. Isacsson, and E. E. B. Campbell, Nano Lett. **12**, 3526 (2012).
[16]S. Scharfenberg, D. Z. Rocklin, C. Chialvo, R. L. Weaver, P. M. Goldbart, and N. Mason, Appl. Phys. Lett. **98**, 091908 (2011).

[17]P. H. Tan, W. P. Han, W. J. Zhao, Z. H. Wu, K. Chang, H. Wang, Y. F. Wang, N. Bonini, N. Marzari, N. Pugno, G. Savini, A. Lombardo, and A. C. Ferrari, Nat. Mater. **11**, 294 (2012).
[18]M. Poot and H. S. J. van der Zant, Appl. Phys. Lett. **92**, 063111 (2008).
[19]S. Cranford, D. Sen, and M. J. Buehler, Appl. Phys. Lett. **95**, 123121 (2009).
[20]X. Chen, L. Zhang, Y. Zhao, X. Wang, and C. Ke, J. Appl. Phys. **116**, 164301 (2014).
[21]K. S. Novoselov, A. K. Geim, S. V. Morozov, D. Jiang, Y. Zhang, S. V. Dubonos, I. V. Grigorieva, and A. A. Firsov, Science **306**, 666 (2004).
[22]P. Nemes-Incze, Z. Osváth, K. Kamarás, and L. P. Biró, Carbon **46**, 1435 (2008).
[23]K. S. Novoselov, D. Jiang, F. Schedin, T. J. Booth, V. V. Khotkevich, S. V. Morozov, and A. K. Geim, Proc. Natl. Acad. Sci. U.S.A. **102**, 10451 (2005).
[24]C. Casiraghi, A. Hartschuh, E. Lidorikis, H. Qian, H. Harutyunyan, T. Gokus, K. S. Novoselov, and A. C. Ferrari, Nano Lett. **7**, 2711 (2007).
[25]Y. Mikata, J. Nanomech. Micromech. **3**, 04013004 (2013).
[26]Y. Zhao, X. Chen, C. Park, C. C. Fay, S. Stupkiewicz, and C. Ke, J. Appl. Phys. **115**, 164305 (2014).
[27]X.-H. Meng, M. Li, Z. Kang, and J.-L. Xiao, Acta Mech. Sin. **30**, 410 (2014).
[28]X. Shi, Q. Yin, and Y. Wei, Carbon **50**, 3055 (2012).
[29]K. N. Kudin, G. E. Scuseria, and B. I. Yakobson, Phys. Rev. B **64**, 235406 (2001).
[30]J. Tersoff, Phys. Rev. B **46**, 15546 (1992).
[31]R. Nicklow, N. Wakabayashi, and H. G. Smith, Phys. Rev. B **5**, 4951 (1972).
[32]C. Q. Ru, Phys. Rev. B **62**, 9973 (2000).
[33]A. Bosak, M. Krisch, M. Mohr, J. Maultzsch, and C. Thomsen, Phys. Rev. B **75**, 153408 (2007).